Inorg. Chem. **2005**, *44*, 7414–7422

Influence of Ligand Rigidity and Ring Substitution on the Structural and Electronic Behavior of Trivalent Iron and Gallium Complexes with Asymmetric Tridentate Ligands

Camille Imbert,[†] Hrant P. Hratchian,[†,§] Mauricio Lanznaster,[†] Mary Jane Heeg,[†] Lew M. Hryhorczuk,[†] Bruce R. McGarvey,[‡] H. Bernhard Schlegel,[†] and Claudio N. Verani*[,†]

Department of Chemistry, Wayne State University, 5101 Cass Ave. Detroit, Michigan 48202, and Department of Chemistry and Biochemistry, University of Windsor, 401 Sunset Ave., Windsor, ON N9B 1P4, Canada

Received April 28, 2005

Species **1**–**6** are $[M^{III}(L)_2]ClO_4$ complexes formed with the PhO^-–CH═N–CH_2–Py imines, $(\mathbf{L}^{I})^-$ and $(\mathbf{L}^{tBuI})^-$, and PhO^-–CH_2–NH–CH_2–Py amines, $(\mathbf{L}^{A})^-$ and $(\mathbf{L}^{tBuA})^-$, in which PhO^- is a phenolate ring and Py is a pyridine ring and the prefix tBu indicates the presence of tertiary butyl groups occupying the positions 4 and 6 of the phenol ring. Monometallic species with d^5 high-spin iron (**1**, **2**, **3**, **4**) and d^{10} gallium (**5, 6)** were synthesized and characterized to assess the influence of the ligand rigidity and the presence of tertiary butyl-substituted phenol rings on their steric, electronic, and redox behavior. Characterization by elemental analysis, mass spectrometry, IR, UV–visible, and EPR spectroscopies, and electrochemistry has been performed, and complexes $[Fe^{III}(L^{tBuI})_2]ClO_4$ **(2)**, $[Fe^{III}(L^{tBuA})_2]ClO_4$ **(4)**, and $[Ga^{III}(L^{tBuI})_2]ClO_4$ **(5)** have been characterized by X-ray crystallography. The crystal structures show the imine ligands meridionally coordinated to the metal centers, whereas the amine ligands are coordinate in a facial mode. Cyclic voltammetry shows that the complexes with the ligands $(\mathbf{L}^{tBuI})^-$ and $(\mathbf{L}^{tBuA})^-$ were able to generate ligand-based phenoxyl radicals, whereas unsubstituted ligands displayed ill-defined redox processes. EPR spectroscopy supports high-spin configurations for the iron complexes. UV–visible spectra are dominated by charge-transfer phenomena, and imine compounds exhibit dramatic hyperchromism when compared to equivalent amines. The tertiary butyl groups on the phenolate ring enhance this trend. Detailed B3LYP/6-31G(d)-level calculations have been used to account for the results observed.

Introduction

In the early 1980s, Kahn demonstrated that the strength of the magnetic coupling between two neighboring metal centers will be influenced by the coordination mode of bidentate and tridentate end-capping amines.[1] More recently, Ziessel et al.[2] have shown that complexes bearing two flexible nitronyl−nitroxide arms can adopt either a meridional or a facial coordination mode, leading to ferro- or antiferromagnetism between the metal center and the radicals. The metal center dictates the coordination mode and leads to cis or trans arrangement of the nitroxide radicals. In both cases, distinct coordination modes foster different interactions between the ligands and the $d_{x^2-y^2}$ and d_{z^2} orbitals of the metal center, leading to modulation of magnetic properties. Thus, it seems reasonable to assume that the use of tridentate $R^1-CH_2-NH-CH_2-R^2$ asymmetric ligands in which R^1 and R^2 indicate different alkyl- or aryl-donor sets will offer distinct ligand fields when end-capping a metal ion. Furthermore, the flexibility of these ligands may lead to preferential meridional or facial coordination modes. These electronic and structural preferences are relevant to the development of catalysts[3,4] and switches[2,5] with unique magnetic and spectroscopic properties. This versatility explains why asymmetric tridentate ligands abound in the literature in which the donor sets R^1/R^2 can be pyridine/thiosemicarbazone,[6]

* To whom correspondence should be addressed. E-mail: cnverani@chem.wayne.edu.
† Wayne State University.
‡ University of Windsor.
§ Present address: Department of Chemistry, Indiana University, Bloomington, IN 47405.

(1) Kahn, O. *Angew. Chem., Int. Ed. Engl.* **1985**, *24*, 834.
(2) Stroh, C.; Belorizky, E.; Turek, P.; Bolvin, H.; Ziessel, R. *Inorg. Chem.* **2003**, *42*, 2938.
(3) Nakayama, Y.; Baba, Y.; Yasuda, H.; Kawakita, K.; Ueyama, N. *Macromolecules* **2003**, *36*; 7953.
(4) Waser, J.; Carreira, E. M. *J. Am. Chem. Soc.* **2004**, *126*, 5676.
(5) Costes, J. P.; Lamere, J. F.; Lepetit, C.; Lacroix, P. G.; Dahan, F.; Nakatani, K.; *Inorg. Chem.* **2005**, *44*, 1973.

10.1021/ic050658j CCC: $30.25
Published on Web 09/21/2005

phenol/amino acids,[7] or phenol/diamino-maleonitrile,[5] among many others. Ligands bearing a σ/π-donor phenol ($-$PhOH) arm and a σ-donor/π-acceptor pyridine ($-$Py) arm have been explored with several metal centers.[8] The presence of phenol-containing arms is particularly relevant because phenoxyl radicals can be generated,[9] meeting current interests in magnetic switches based on electroactive ligands.[10] The introduction of substituents in the 4 and 6 positions of the phenol ring leads to steric or electronic effects, and upon deprotonation, the phenolato ring decreases the overall charge, lowering the number of counterions needed for charge balance. The use of structurally related asymmetric imines PhOH$-$CH$_2-$N$=$CH$_2-$Py could represent a way of increasing the rigidity of the ligands, thus fostering a preferential meridional geometry.

On the basis of these premises and aiming at understanding the factors governing the geometric preferences of the imine and amine ligands in respective $[M^{III}(PhO^{-}-CH_2-N{=}CH_2-Py)_2]^+$ and $[M^{III}(PhO^{-}-CH_2-NH-CH_2-Py)_2]^+$ species, complexes of iron(III) and gallium(III) were synthesized (Scheme 1). We are particularly interested in understanding how the ligand rigidity and the presence of substituted phenolate rings relate to the steric, electronic, electrochemical, and magnetic behavior of these complexes because they serve as archetypes of soft materials currently under development in our labs. In this work we demonstrate by means of three crystallographic structures obtained for **2**, **4**, and **5** that the asymmetric amines tend toward facial coordination, whereas equivalent imines adopt meridional coordination. In addition, we compare the spectroscopic properties of similar ligands when coordinated to different metal ions and we study the redox chemistry of these species. The experimental observations corroborate with computational work, and the results allow the postulation of relationships between molecular geometry and physical properties.

Scheme 1

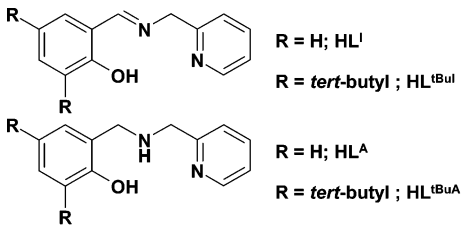

$[Fe^{III}(L^{I})_2]ClO_4\cdot H_2O$ **(1)** $[Fe^{III}(L^{tBuA})_2]ClO_4\cdot CH_3OH$ **(4)**
$[Fe^{III}(L^{tBuI})_2]ClO_4$ **(2)** $[Ga^{III}(L^{tBuI})_2]ClO_4$ **(5)**
$[Fe^{III}(L^{A})_2]ClO_4$ **(3)** $[Ga^{III}(L^{tBuA})_2]ClO_4\cdot CH_3OH$ **(6)**

Experimental Section

1. Materials and Methods. Unless otherwise noted, reagents and solvents were used as received from commercial sources. Dichloromethane and acetonitrile were doubly purified using alumina columns in a solvent purification system from Innovative Technologies, and methanol was distilled over CaH_2. Infrared spectra were measured from 4000 to 400 cm^{-1} as KBr pellets on a Tensor 27 FTIR spectrophotometer. ^{1}HNMR spectra were measured using Varian 300 and 400 mHz instruments. ESI(positive) spectra were measured in either a triple quadrupole Micromass QuattroLC or in a single quadrupole Waters ZQ2000 mass spectrometer with an electrospray/APCI or ESCi source. Experimental assignments were simulated on the basis of peak position and isotopic distributions. Elemental analyses were performed by Midwest Microlab, Indianapolis, IN. UV$-$visible spectroscopy from 1.0×10^{-4} dichoromethane and acetonitrile solutions were performed using a Cary 50 spectrometer in the range 250$-$1100 nm. Cyclic voltammetry experiments were performed using a BAS 50W voltammetric analyzer. A standard three-electrode cell was employed with a glassy-carbon working electrode, a Pt-wire auxiliary electrode, and an Ag/AgCl reference electrode under an inert atmosphere at room temperature (RT). Potentials are presented vs Fc^+/Fc[11] as the internal standard. First-derivative X-Band EPR spectra of 1.0×10^{-3} M acetone solutions of selected compounds were performed with a Bruker ESP 300 spectrometer at 115 K using liquid nitrogen as the coolant.

2. X-Ray Structural Determinations for 2, 4, and 5. Diffraction data for compounds **2** and **4** were collected on a Bruker P4/CCD diffractometer equipped with Mo radiation and a graphite monochromator at either RT (for **2**) or 213 K (compound **4**). All data were processed using SMART, SAINT, SADABS, APEX II,[12] and SHELX-97[13] software. Typical *tert*-butyl disorder was observed in **2** (Table 1), and partial atomic occupancies were used in the model. Large thermal ellipsoids are also evident for the perchlorato oxygen atoms of **2**. In **4**, the perchlorate oxygen atoms were too disordered to refine reasonably. Both the perchlorate anion and the methanol solvent were placed by use of Spek's SQUEEZE portion of the PLATON software.[14] Diffraction data for **5** were collected on a Bruker APEX II diffractometer equipped with Mo Kα radiation

(6) García-Tojal, J.; Donnadieu, B.; Costes, J. P.; Serra, J. L.; Lezama, L.; Rojo, T. *Inorg. Chim. Acta* **2002**, *333*, 132.
(7) (a) Scarpellini, M.; Neves, A.; Bortoluzzi, A. J.; Vencato, I.; Drago, V.; Ortiz, W. A.; Zucco, C. *Dalton Trans.* **2001**, 2616. (b) Toyota, E.; Ng, K. K. S.; Sekizaki, H.; Itoh, K.; Tanizawa, K.; James, M. N. G. *J. Mol. Biol.* **2001**, *305*, 2001. (c) Jursik, F.; Archer, R. D. *Collect. Czech. Chem. Commun.* **1995**, *60*, 2097. (d) Casella, L.; Gullotti, M.; Pintar, A.; Messori, L.; Rockenbauer, A.; Gyor, M. *Inorg. Chem.* **1987**, *26*, 1031. (e) Burrows, R. C.; Bailar, J. C., Jr. *J. Am. Chem. Soc.* **1966**, *88*, 4150.
(8) (a) Motoyama, T.; Shimazaki, Y.; Yajima, T.; Nakabayashi, Y.; Naruta, Y.; Yamauchi, O. *J. Am. Chem. Soc.* **2004**, *126*, 7378. (b) Mondal, A.; Sarkar, S.; Chopra, D.; Row: T. N.; Rajak, K. K. *Dalton Trans.* **2004**, 3244. (c) Drechsel, S. M.; Kaminski, R.; Nakagaki, S.; Wypych, F. *J. Colloid Interface Sci.* **2004**, *277*, 138. (d) Baruah, B.; Das, S.; Chakravorty, A. *Inorg. Chem.* **2002**, *41*, 4502. (e) Cameron, P. A.; Gibson V. C.; Redshaw, C.; Segal, J. A.; Bruce, M. D.; White, A. J. P.; William., D. J. *Chem. Commun.* **1999**, *18*, 1883. (f) Neves, A.; Verani, C. N.; Brito, M. A.; Vencato, I.; Mangrich, A.; Oliva, G.; Dulce D. H.; Souza. F.; Batista, A. A. *Inorg. Chim. Acta* **1999**, *290*, 207. (g) Abrahams, A.; Bandoli, G.; Gatto, S.; Gerber, T. I. A.; Du Preez, J. G. H. *J. Coord. Chem.* **1997**, *42*, 303. (h) Hatfield, W. E.; Bunger, F. L. *Inorg. Chem.* **1969**, *08*, 1194.
(9) (a) Thomas, F.; Gellon, G.; Gautier-Luneau, I.; Saint-Aman, E.; Pierre, J. L. *Angew. Chem., Int. Ed.* **2002**, *41*, 3047. (b) Shimazaki, Y.; Huth, S.; Odani, A.; Yamauchi, O. *Angew. Chem., Int. Ed.* **2000**, *39*, 1666. (c) Philibert, A.; Thomas, F.; Philouze, C.; Hamman, S.; Saint-Aman, E.; Pierre, J. L. *Chem. Eur. J.* **2003**, *09*, 3803. (d) Itoh, S.; Takayama, S.; Arakawa, R.; Furuta, A.; Komatsu, M.; Ishida, A.; Takamuku, S.; Fukuzumi, S. *Inorg. Chem.* **1997**, *36*, 1407. (e) Jazdzewski, B. A.; Tolman, W. B. *Coord. Chem. Rev.* **2000**, *200*$-$*202*, 633. (f) Hockertz, J.; Steenken, S.; Wieghardt, K.; Hildebrandt, P. *J. Am. Chem. Soc.* **1993**, *115*, 11222.
(10) (a) Dei, A.; Gatteschi, D.; Sangregorio, C.; Sorace, L. *Acc. Chem. Res.* **2004**, *37*, 828.
(11) Gagne, R.; Koval, C.; Licenski, G. *Inorg. Chem.* **1980**, *19*, 2854.
(12) APEX II, SMART, SAINT and SADABS collection and processing programs are distributed by the manufacturer. Bruker AXS, Inc., Madison, WI.
(13) Sheldrick, G. *SHELX-97*; University of Göttingen: Göttingen, Germany, 1997.
(14) (a) Spek, A. L. *PLATON*; Utrecht University: Utrecht, The Netherlands, 2003. (b) Spek, A. L. *J. Appl. Crystallogr.* **2003**, *36*, 7.

Table 1. Crystal Data for **2**, **4**, and **5**[a]

	$[Fe^{III}(\mathbf{L}^{tBuI})_2]ClO_4$ **(2)**	$[Fe^{III}(\mathbf{L}^{tBuA})_2]ClO_4 \cdot CH_3OH$ **(4)**	$[Ga^{III}(\mathbf{L}^{tBuI})_2]ClO_4$ **(5)**
formula	$C_{42}H_{54}ClFeN_4O_6$	$C_{43}H_{62}ClFeN_4O_7$	$C_{42}H_{54}ClGaN_4O_6$
fw	802.19	838.27	816.06
space group	*P*2(1)/*c*	*Pnma*	*P*2(1)/*c*
a (Å)	20.713(2)	19.827(4)	20.4420(6)
b (Å)	11.2652(13)	37.450(9)	11.2287(3)
c (Å)	21.123(2)	12.556(2)	20.8587(5)
β (deg)	118.9832	90	118.7080(10)
V (Å^3)	4311.5(8)	9324(3)	4199.32(19)
Z	4	8	4
temp (K)	295(2)	213(2)	100(2)
λ (Å)	0.71073	0.71073	0.71073
ρ, calcd (g cm^{-3})	1.236	1.194	1.291
μ (mm^{-1})	0.460	0.430	0.769
$R(F)$(%)	6.21	8.00	3.62
$R_w(F)$ (%)	16.44	21.36	10.05

[a] $R(F) = \sum||F_o| - |F_c||/\sum|F_o|$ $R_w(F) = [\sum w(F_o^2 - F_c^2)^2/\sum w(F_o^2)^2]^{1/2}$.

and graphite monochromator at 100 K. Two sets of partial-occupancy methyl groups were placed on C35 (*tert*-butyl) in an 80/20 distribution. The minor component set (20%) was held isotropic.

3. Electronic Structure Calculations. The B3LYP/6-31G(d) level of theory[15] was employed throughout, and all calculations were done using the GAUSSIAN series of programs.[16] Geometries were fully minimized, without symmetry constraints, using standard methods.[17] Located stationary points were characterized by computing analytic vibrational frequencies. Reported energies include zero-point correction. Cartesian coordinates of all optimized structures are provided as Supporting Information.

4. Syntheses. The ligands $\mathbf{HL}^{I}$ (2-hydroxybenzyl-2-pyridylmethyl)imine, $\mathbf{HL}^{tBuI}$ (2-hydroxy-4−6-di-*tert*-butylbenzyl-2-pyridylmethyl)imine, $\mathbf{HL}^{A}$ (2-hydroxybenzyl-2-pyridylmethyl)amine, and $\mathbf{HL}^{tBuA}$ (2-hydroxy-4−6-di-*tert*-butylbenzyl-2-pyridylmethyl)amine were synthesized according to the literature.[18−21] General pathways are described in the syntheses of the iron and gallium complexes. **Caution**: *Although no difficulties were experienced, complexes* ***1−6*** *were isolated as their perchlorate salts, and therefore, they should be handled as potentially explosive compounds.*

4.1. Iron Complexes. A 10 mL MeOH solution of $Fe(ClO_4)_3 \cdot 9H_2O$ (0.52 g; 1.0 mmol) was added dropwise to a 30 mL MeOH solution containing 2.0 mmol of the appropriate ligand and Et_3N (0.28 mL; 2.0 mmol). The resulting solutions changed color (dark red for $\mathbf{HL}^{I}$ and $\mathbf{HL}^{tBuI}$, violet for $\mathbf{HL}^{A}$, and dark blue for $\mathbf{HL}^{tBuA}$) and were gently refluxed for 1 h, when they were filtered while warm and concentrated to one-third of the original volume to render amorphous solids. The compounds were crystallized in methanol at room temperature by slow evaporation of the solvent giving microcrystalline precipitates.

4.1.1. $[Fe^{III}(L^{I})_2]ClO_4 \cdot H_2O$ (1). Yield = 82%. Anal. Calcd for $[C_{26}H_{24}N_4\ Cl_1O_7Fe_1]$: C, 52.41, H, 3.84, N 9.40. Found: C, 52.43, H, 3.75, N 8.97%. IR (KBr, cm^{-1}) 1096 (ν_{Cl-O}), 1616 ($\nu_{C=N}$), 3300−3320 (ν_{OH}). ESI pos. in MeOH: $m/z = 478.1$ for $[Fe^{III}(\mathbf{L}^{I})_2]^+$.

4.1.2. $[Fe^{III}(L^{tBuI})_2]ClO_4$ (2). The reddish microcrystalline precipitate was successively recrystallized in methanol affording X-ray quality crystals. Yield = 87%. Anal. Calcd for $[C_{42}H_{54}N_4\ Cl_1O_6Fe_1]$: C, 62.88, H, 6.78, N 6.98. Found: C, 62.93, H, 6.89, N 6.89%. IR (KBr, cm^{-1}) 1095 (ν_{ClO4}), 1611 ($\nu_{C=N}$), 2868−2953 (ν_{C-H} from *tert*-butyl groups). ESI pos. in MeOH: $m/z = 702.13$ for $[Fe^{III}(\mathbf{L}^{tBuI})_2]^+$.

4.1.3. $[Fe^{III}(L^{A})_2]ClO_4$ (3). This compound is highly deliquescent, and several attempts to isolate a microcrystalline sample failed. Thus, the identity of the compound is based on its mass and infrared analysis. Yield ≈ 69%. IR (KBr, cm^{-1}) 1088 (ν_{Cl-O}), 3418 (ν_{O-H} broad); ESI pos. in MeOH: $m/z = 482.13$ for $[Fe^{III}(\mathbf{L}^{A})_2]^+$.

4.1.4. $[Fe^{III}(L^{tBuA})_2]ClO_4 \cdot CH_3OH$ (4). The microcrystalline dark blue precipitate was recrystallized in methanol affording crystals

(15) (a) Becke, A. D. *Phys. Rev. A* **1988**, *38*, 3098. (b) Becke, A. D. *J. Chem. Phys.* **1993**, *98*, 5648. (c) Lee, T.; Yang, W. T.; Parr, R. G. *Phys. Rev. B* **1988**, *37*, 785. (d) Ditchfield, R.; Hehre, W. R.; Pople, J. A. *J. Chem. Phys.* **1971**, *54*, 724. (e) Gordon, M. S. *Chem. Phys. Lett.* **1980,** *76*, 163. (f) Hariharan, P. C.; Pople, J. A. *Theor. Chim. Acta* **1973**, *28*, 213. (g) Hariharan, P. C.; Pople, J. A. *Mol. Phys.* **1974**, *27*, 209. (h) Hehre, W. R.; Ditchfield, R.; Pople, J. A. *J. Chem. Phys.* **1972**, *56*, 225.

(16) Frisch, M. J.; Trucks, G. W.; Schlegel, H. B.; Scuseria, G. E.; Robb, M. A.; Cheeseman, J. R.; Montgomery, J. A., Jr.; Vreven, T.; Kudin, K. N.; Burant, J. C.; Millam, J. M.; Iyengar, S. S.; Tomasi, J.; Barone, V.; Mennucci, B.; Cossi, M.; Scalmani, G.; Rega, N.; Petersson, G. A.; Nakatsuji, H.; Hada, M.; Ehara, M.; Toyota, K.; Fukuda, R.; Hasegawa, J.; Ishida, M.; Nakajima, T.; Honda, Y.; Kitao, O.; Nakai, H.; Klene, M.; Li, X.; Knox, J. E.; Hratchian, H. P.; Cross, J. B.; Bakken, V.; Adamo, C.; Jaramillo, J.; Gomperts, R.; Stratmann, R. E.; Yazyev, O.; Austin, A. J.; Cammi, R.; Pomelli, C.; Ochterski, J. W.; Ayala, P. Y.; Morokuma, K.; Voth, G. A.; Salvador, P.; Dannenberg, J. J.; Zakrzewski, V. G.; Dapprich, S.; Daniels, A. D.; Strain, M. C.; Farkas, O.; Malick, D. K.; Rabuck, A. D.; Raghavachari, K.; Foresman, J. B.; Ortiz, J. V.; Cui, Q.; Baboul, A. G.; Clifford, S.; Cioslowski, J.; Stefanov, B. B.; Liu, G.; Liashenko, A.; Piskorz, P.; Komaromi, I.; Martin, R. L.; Fox, D. J.; Keith, T.; Al-Laham, M. A.; Peng, C. Y.; Nanayakkara, A.; Challacombe, M.; Gill, P. M. W.; Johnson, B.; Chen, W.; Wong, M. W.; Gonzalez, C.; Pople, J. A. *Gaussian 03*; Gaussian, Inc.: Wallingford, CT, 2004.

(17) Schlegel, H. B. *J. Comput. Chem.* **1982**, *3*, 214.

(18) For references on $\mathbf{HL}^{I}$, see: Baruah, B.; Rath, S.; Chakravorty, A. *Eur. J. Inorg. Chem.* **2004**, *09*, 1873. (b) Lambi, E.; Gegiou, D.; Hadjoudis, E. *J. Photochem. Photobiol. A* **1995**, *86*, 241.

(19) For references on $\mathbf{HL}^{A}$, see: (a) Horn, A.; Vencato, I.; Bortoluzzi, A. J.; Hoerner, R.; Silva, R. A., Nome, F.; Spoganicz, B.; Drago, V.; Terenzi, H.; de Oliveira, M. C. B.; Werner, R.; Haase, W.; Neves, A. *Inorg. Chim. Acta* **2005**, *358*, 339. (b) Johansson, A.; Abrahamsson, M.; Magnuson, A.; Huang, P.; Maartensson, J.; Styring, S.; Hammarström, L.; Sun, L.; Åkermark, B. *Inorg. Chem.* **2003**, *42*, 7502. (c) Lomoth, R.; Huang, P.; Zheng, J.; Sun, L.; Hammarström, L.; Åkermark, B.; Styring, S. *Eur. J. Inorg. Chem.* **2002**, 2965. (d) Menage, S.; Gellon, G.; Pierre, J.-L.; Zurita, D.; Saint-Aman, E. *Bull. Soc. Chim. France* **1997**, *134*, 785. (e) Neves, A.; de Brito, M. A.; Vencato, I.; Drago, V.; Griesar, K.; Haase, W. *Inorg. Chem.* **1996**, *35*, 2360. (f) Viswanathan, R.; Palaniandavar, M.; Balasubramanian, T.; Muthiah, P. T. *J. Chem. Soc. Dalton Trans.* **1996**, 2519. (g) Krebs, B.; Schepers, K.; Bremer, B.; Henkel, G.; Althaus, E.; Mueller-Warmuth, W.; Griesar, K.; Haase, W. *Inorg. Chem.* **1994**, *33*, 1907. (h) Uma, R.; Viswanathan, R.; Palaniandavar, M.; Lakshminarayanan, M. *Dalton Trans.* **1994**, 1219. (f) Neves, A.; de Brito, M. A.; Vencato, I.; Drago, V.; Griesar, K.; Haase, W.; Mascarenhas, Y. P. *Inorg. Chim. Acta* **1993**, *214*, 05.

(20) For references on $\mathbf{HL}^{tBuI}$, see: (a) Reference 3. (b) Cameron, P. A.; Gibson, V. C.; Redshaw, C.; Segal, J. A.; White, A. J. P.; Williams, D. J. *Dalton Trans.* **2002,** *3*, 415.

(21) For references on $\mathbf{HL}^{tBuA}$, see: (a) Mitchell, J. M.; Finney, N. S. *J. Am. Chem. Soc.* **2001**, *123*, 862. (b) Wong, Y.-L.; Yan, Y.; Chan, E. S.; Yang, Q.; Mak, T. C.; Ng, D. K. *Dalton Trans.* **1998**, 3057.

suitable for X-ray analysis. Yield = 84%. Anal. Calcd for $[C_{43}H_{62}N_4Cl_1O_7Fe_1]\cdot CH_3OH$: C, 60.08, H, 7.50, N 6.52. Found: C, 59.49, H, 7.48, N 6.47%. IR (KBr, cm^{-1}) 1077 (ν_{Cl-O}), 2867−2950 (ν_{C-H}), 3283 (ν_{N-H}), 3449 (ν_{O-H}). ESI pos. in MeOH: m/z = 706.34 for $[Fe^{III}(\mathbf{L}^{tBuA})_2]^+$.

4.2. Gallium Complexes. Inside a glovebox, a solid sample of anhydrous $GaCl_3$ (0.18 g; 1.0 mmol) was added to a 30 mL dry MeOH solution containing 2.0 mmol of the appropriate ligand and Et_3N (0.28 mL; 2.0 mmol). The resulting yellowish solutions were stirred at RT for 1 h. Filtration to isolate any solid material was followed by counterion exchange by the addition of 1.0 mmol of $NaClO_4$. After 24 h, dark yellow microcrystalline solids were isolated via frit filtration. The isolated precipitates were washed with small portions of cold methanol and ethyl ether.

4.2.1. $[Ga^{III}(L^{tBuI})_2]ClO_4$ (5). The yellowish microcrystalline compound was successively recrystallized in methanol to afford crystals suitable for X-ray diffractometry. Yield = 92%. Anal. Calcd for $[C_{42}H_{54}N_4Cl_1O_6Ga_1]$: C, 61.81, H, 6.67, N 6.87. Found: C, 62.09, H, 6.66, N 6.80%. IR (KBr, cm^{-1}) 1094 (ν_{Cl-O}), 1624 ($\nu_{C=N}$), 2869−2958 (ν_{C-H}). ESI pos. in MeOH: m/z = 715.29 for $[Ga^{III}(\mathbf{L}^{tBuI})_2]^+$.

4.2.2. $[Ga^{III}(L^{tBuA})_2]ClO_4\cdot CH_3OH$ (6). Yield = 80%. Anal. Calcd for $[C_{43}H_{62}N_4Cl_1O_7Ga_1]$: C, 60.60, H, 7.31, N 6.57. Found: C, 60.97, H, 7.06, N 6.49%. IR (KBr, cm^{-1}) 1098 (ν_{Cl-O}), 2867−2952 (ν_{C-H}), 3444 (ν_{O-H}). ESI pos. in MeOH: m/z = 719.4 for $[Ga^{III}(\mathbf{L}^{tBuA})_2]^+$.

Results and Discussion

1. Synthetic Approach. Schiff condensation of aminomethylpyridine with the appropriate aldehyde in methanol generates the imine ligands, and reduction with $NaBH_4$ gives the amines. An article on $[Fe(\mathbf{L}^{tBuA})Cl_2]$ as a polymer catalyst[21b] does not provide structural, spectroscopic, or redox data, otherwise useful for comparisons. All ligands gave yields between 85 and 95% and were characterized by ^1H NMR and infrared spectroscopies and ESI mass spectrometry. Complexes **1**, **2**, **3**, and **4** were synthesized by treating the respective ligands with hydrated ferric perchlorate (eq 1). Complexes **5** and **6** were obtained with gallium chloride in dry methanol followed by counterion metathesis with sodium perchlorate (eqs 2 and 3).

$$2H\mathbf{L}^{I/A} + Fe(ClO_4)_3\cdot 9H_2O + 2Et_3N \xrightarrow{MeOH} [Fe(\mathbf{L}^{I/A})_2]ClO_4 + 2(Et_3NH)ClO_4 + 9H_2O \quad (1)$$

$$2H\mathbf{L}^{tBuI/A} + GaCl_3 + 2Et_3N \xrightarrow{MeOH} [Ga(\mathbf{L}^{tBuI/A})_2]Cl + 2(Et_3NH)Cl \quad (2)$$

$$[Ga(\mathbf{L}^{tBuI/A})_2]Cl + NaClO_4 \xrightarrow{MeOH} [Ga(\mathbf{L}^{tBuI/A})_2]ClO_4 + NaCl \quad (3)$$

These reactions yielded pseudo-octahedral mononuclear species in which one metal is surrounded by two tridentate ligands with R being H or *tert*-butyl groups.

2. Infrared Spectroscopy, Mass Spectrometry, and Elemental Analysis. The imine ligands show a C=N peak at 1630 cm^{-1} that shifts upon coordination. The tertiary butyl groups from $\mathbf{HL}^{tBuI}$ and $\mathbf{HL}^{tBuA}$ are seen as $-CH_3$ stretches between 2950 and 2870 cm^{-1}, and perchlorate counterions are found between 1116 and 1088 cm^{-1}. ESI mass spectrometry in the positive mode in methanol gave single, well-defined peaks corresponding to $m/z = [M^{III}(\mathbf{L})_2]^+$ (100%) for all complexes. These peaks were simulated and show good agreement in their position and isotopic distributions, as shown in Figure 1. Other peaks present displayed intensity below 1%.

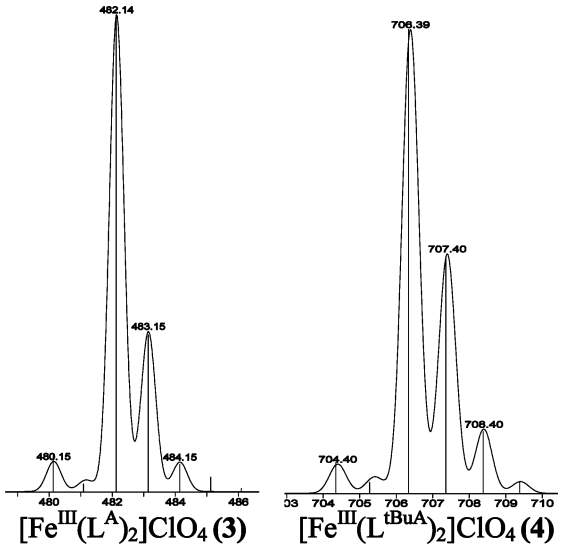

Figure 1. Experimental and simulated ESI(positive) peaks for complexes **3** (m/z = 480, 481, 482, 483, 484, 485) and **4** (m/z = 704, 705, 706, 707, 708, 709).

Good elemental analyses were obtained for **1**, **2**, **4**, **5**, and **6**. Compound **3** is deliquescent, and several attempts to isolate a microcrystalline sample with different counterions failed. We had difficulty following the protocol available in the literature,[19f] and the use of anhydrous $FeCl_3$ under inert conditions gave a methoxy/chloro-bridged dimer.[22] The identity of **3** is based on its mass and isotopic distribution, IR, and UV−visible spectra.

3. Molecular Structures. The structure of HL^A has been published elsewhere.[8f] Complexes **2**, **4**, and **5** have had their structures determined, with the ORTEP diagrams shown in Figure 2a−c. Table 2 summarizes selected bond lengths and angles for these complexes.

3.1. $[Fe^{III}(L^{tBuI})_2]ClO_4$ (2). This complex consists of discrete monometallic molecules composed of the iron(III) ion surrounded by two deprotonated ligands $(L^{tBuI})^-$ arranged in a pseudo-octahedral environment described as $[Fe<N_{im1}N_{im2}><N_{py1}O_{(phO-)1}><N_{py2}O_{(phO-)2}>]$. The notation $<A_1B_2>$[23] indicates that A is trans to B, with A and B corresponding to the pyridine (N_{py}), imine (N_{im}), amine (N_{am}), or phenolato (O_{phO-}) groups. Subscripts 1 and 2 designate the first or the second ligand. The ORTEP diagram of **2** is shown in Figure 2a, indicating that both ligands are coordinated in a meridional fashion. Each ligand coordinates to the metal by an NN′O donor set via an amine and a pyridine nitrogen atom, as well as by the oxygen atom of the phenolate group. Short bonds are exhibited at C(7)−N(1) and C(28)−N(3) (1.29 Å) and corroborate with the imine nature of the ligand. The average distances are 2.10 Å for Fe−N_{im}, 2.20 Å for Fe−N_{py}, and 1.89 Å for Fe−O_{phO-}, as expected for a high-spin Fe(III)

(22) Kaminski, R.; Flörke, U.; Drechsel, S. unpublished results.
(23) Adapted from Miessler, G.L; Tarr, D. A. *Inorganic Chemistry*; Pearson-Prentice Hall: Upper Saddle River, NJ, 2004; pp 311−315.

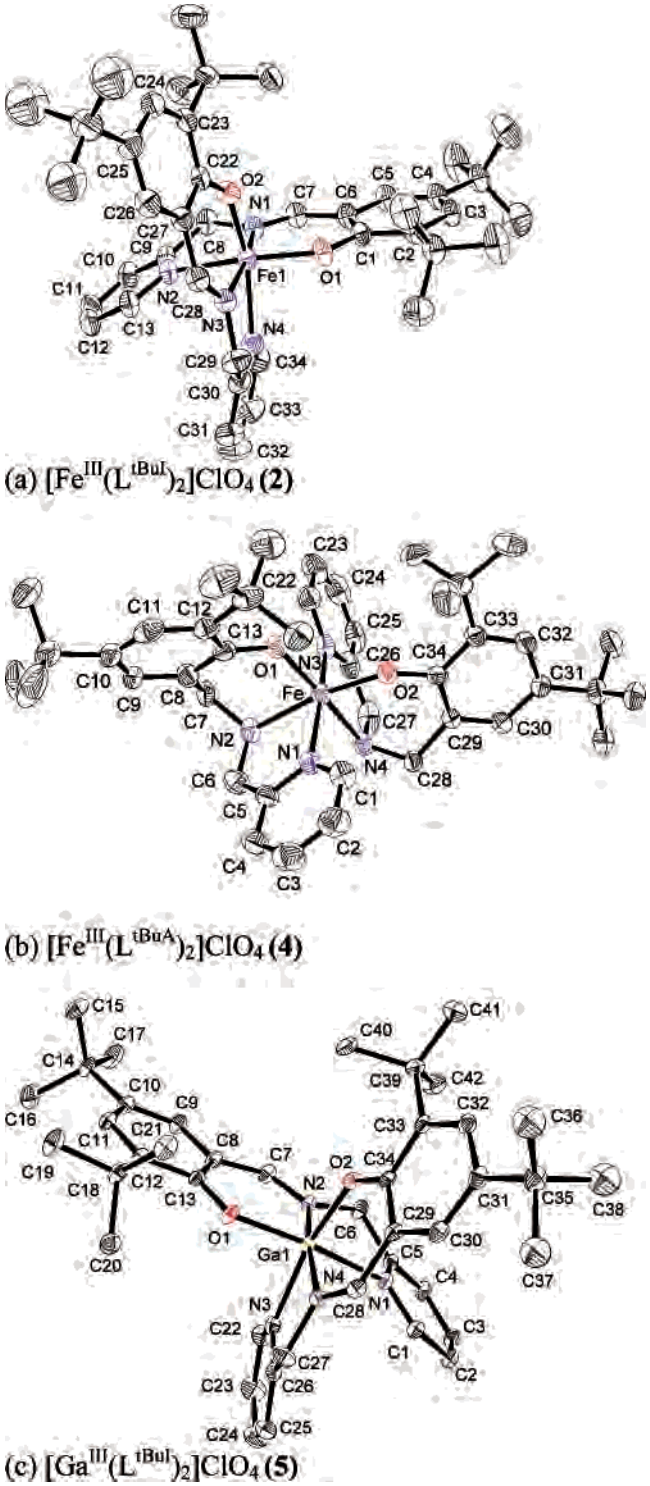

Figure 2. ORTEP diagrams at 50% probability for **2**, **4**, and **5**. Counterions, solvents, and hydrogen atoms are excluded for clarity.

ion.[24] The meridional coordination of each ligand leads to a cis orientation of the two pyridines with an angle N(2)−Fe−N(4) of 79.4°. Similarly, the two phenolate rings are cis to each other with an O(1)−Fe−O(2) angle of 97.7°. The trans imine nitrogen atoms display an N(1)−Fe−N(3) angle of 168.6°. The angles between the phenolate rings and the iron center given by C(1)−O(1)−Fe(1) = 137.5° and C(22)−O(2)−Fe(1) = 136.4° are slightly above the expected range from 130 to 135°.[25] A disordered perchlorate counterion is also present.

3.2. $[Fe^{III}(L^{tBuA})_2]ClO_4 \cdot CH_3OH$ (4). Discrete mononuclear molecules of **4** show one iron(III) center coordinated to two deprotonated $(\mathbf{L}^{tBuA})^-$ ligands with a set of donors $N_{am}N_{py}O_{phO-}$ in a pseudo-octahedral environment (Figure 2b). The C=N bonds present in complexes **2** and **5** are substituted by the longer bonds N(2)−C(7) = 1.47 Å and N(4)−C(28) = 1.48 Å, indicating their amine nature. Both ligands are facially coordinated, with the two pyridine rings trans to one another (Fe−N_{av} = 2.13 Å). The oxygen atoms of the phenolate rings (Fe−O_{av} = 1.87 Å), and the amine nitrogen atoms (Fe−N_{av} = 2.21 Å) are occupying cis positions in the basal plane, typical values for coordination of such ligands to an iron(III) ion. Complex **4** is described as $[Fe<N_{am1}O_{(phO-)2}> <N_{am2}O_{(phO-)1}> < N_{py1}N_{py2},>]$. The angles between the phenolate rings and the iron center given by C(13)−O(1)−Fe(1) = 132.5° and C(34)−O(2)−Fe(1) = 134.7° fit well within the expected range, as discussed for **2**. Interestingly, this geometry closely resembles that of the complex $[Fe^{III}(bbpen)]NO_3 \cdot CH_3OH$ [26] in which the ligand $(bbpen)^{2-}$ is equivalent to two $(\mathbf{L}^{A})^-$ units tethered by an ethylenediamine bridge. Similarly, the same approximation gives **5** C_{2v} symmetry. A disordered counterion perchlorate and a molecule of methanol complete the description of the lattice contents.

3.3. $[Ga^{III}(L^{tBuI})_2]ClO_4$ (5). Discrete monometallic molecules composed by two deprotonated ligands $(\mathbf{L}^{tBuI})^-$ meridionally coordinated to the gallium(III) ion describe complex **5**. The arrangement is given as $[Ga<N_{im1}N_{im2}> <N_{py1}O_{(phO-)1}> <N_{py2}O_{(phO-)2}>]$ (Figure 2c). Interestingly, this ion shows shorter distances than **2**. Structural data on gallium(III) ions coordinated to phenolate rings is limited, but the values above relate well with available information.[27h] The geometry adopted by **5** does not resemble that for $[Ga^{III}$-(Clbbpen)$]ClO_4$ because the pyridine rings are trans to each other. C_{2v} symmetry is also observed for this system.

3.4. *Meridional* vs *Facial* Coordination of the Ligands. The evidence offered by these structures supports that imine ligands coordinate meridionally while amines prefer facial modes. For **4**, an increase of 0.10 Å in the distance Fe−N_{am} is observed when compared to the distance Fe−N_{im} in **2**. This increase is associated with an equivalent decrease in the distance Fe−N_{py}, whereas the metal-to-phenolate distance remains unchanged. The differences appear to be related to the less rigid nature of the amine ligand. It is possible to postulate that the imine ligands $(\mathbf{L}^{I})^-$ and $(\mathbf{L}^{tBuI})^-$ are more rigid coordinating in a meridional mode, whereas the amine ligands $(\mathbf{L}^{A})^-$ and $(\mathbf{L}^{tBuA})^-$ can accommodate a facial mode. Imine ligands as in **2** and **5** preclude trans-phenolates due to steric constraints, but cis and trans-coordination modes are allowed for amine complexes **4** and **6**. To have a full

(24) Hwang, J. W.; Govindaswamy, K.; Koch, S. A. *Chem. Commun.* **1998**, 1667.

(25) (a) Holm, R. H.; Kennepohl, P.; Solomon, E. I. *Chem. Rev.* **1996**, *96*, 2239. (b) Solomon, E. I.; Brunold, T. C.; Davis, M. I.; Kemsley, J. N.; Lee, S. K.; Lehnert, N.; Neese, F.; Skulan, A. J.; Yang, Y. S.; Zhou, *J. Chem. Rev.* **2000**, *100*, 235.

(26) (a) Setyawati, I. A.; Rettig, S. J.; Orvig, C. *Can. J. Chem.* **1999**, *77*, 2033. (b) Davis, J. C.; Kung, W. J.; Averill, B. A. *Inorg. Chem.* **1986**, *25*, 394.

Table 2. Selected Bond Distances (Å) and Angles (deg) for **2**, **4**, and **5**

$[Fe^{III}(\mathbf{L}^{tBuI})_2]ClO_4$ **(2)**		$[Fe^{III}(\mathbf{L}^{tBuA})_2]ClO_4 \cdot CH_3OH$ **(4)**		$[Ga^{III}(\mathbf{L}^{tBuI})_2]ClO_4$ **(5)**	
Fe(1)−O(1)	1.887(2)	Fe(1)−O(2)	1.868(3)	Ga(1)−O(1)	1.8999(10)
Fe(1)−O(2)	1.895(2)	Fe(1)−O(1)	1.878(3)	Ga(1)−O(2)	1.9024(10)
Fe(1)−N(1)	2.095(2)	Fe(1)−N(1)	2.140(4)	Ga(1)−N(2)	2.0041(11)
Fe(1)−N(3)	2.106(2)	Fe(1)−N(3)	2.124(4)	Ga(1)−N(4)	2.0170(11)
Fe(1)−N(2)	2.201(3)	Fe(1)−N(2)	2.210(3)	Ga(1)−N(1)	2.1781(11)
Fe(1)−N(4)	2.195(3)	Fe(1)−N(4)	2.223(3)	Ga(1)−N(3)	2.1591(12)
O(1)−C(1)	1.314(3)	C(13)−O(1)	1.360(5)	C(13)−O(1)	1.3146(15)
O(2)−C(22)	1.314(3)	C(34)−O(2)	1.349(5)	C(34)−O(2)	1.3157(15)
C(7)−N(1)	1.293(4)	N(2)−C(7)	1.474(5)	N(2)−C(7)	1.2989(17)
C(28)−N(3)	1.293(4)	N(4)−C(28)	1.481(5)	N(4)−C(28)	1.2958(17)
N(1)−C(8)	1.460(4)	C(6)−N(2)	1.468(6)	C(6)−N(2)	1.4661(18)
N(3)−C(29)	1.458(4)	C(27)−N(4)	1.500(6)	C(27)−N(4)	1.4615(19)
N(1)−Fe(1)-N(3)	168.60(11)	N(3)−Fe(1)-N(1)	161.99(14)	N(2)−Ga(1)-N(4)	169.93(5)
O(2)−Fe(1)-N(4)	160.84(9)	O(2)−Fe(1)-N(2)	171.04(13)	O(2)−Ga(1)-N(3)	166.95(4)
O(1)−Fe(1)-N(2)	158.97(9)	O(1)−Fe(1)-N(4)	170.52(12)	O(1)−Ga(1)-N(1)	165.26(4)
C(1)−O(1)-Fe(1)	137.5(2)	C(13)−O(1)-Fe(1)	132.5(3)	C(13)−O(1)-Ga(1)	130.96(9)
C(22)−O(2)-Fe(1)	136.4(2)	C(34)−O(2)-Fe(1)	134.7(3)	C(34)−O(2)-Ga(1)	131.17(9)

understanding of the *mer*/*fac* and cis/trans geometric preferences observed in these complexes, computational calculations to the B3LYP/6-31G(d) level of theory were performed and will be discussed later in this paper.

4. Electronic Spectroscopy. The electronic spectra of the ligands and complexes were measured in dichloromethane to compare differences between imine and amine ligands, as well as the influence of the bulky electron-donating *tert*-butyl groups in the phenolate rings. Figure 3 shows sets of spectra useful for the comparisons below and Table 3 summarizes the data.

Both $\mathbf{HL}^{A}$ and $\mathbf{HL}^{tBuA}$ show intraligand $\pi \rightarrow \pi^*$ bands at 262 and 268 nm ($\epsilon \approx 4000$ L mol^{-1} cm^{-1} per band), and similar intensities suggest a 1:1 ratio for the pyridine and phenolate moieties.[8f] No transitions were observed in the visible region. The imine ligands exhibit dramatic hyperchromism when compared to the amines; the 262 nm band and 268 nm shoulder are 2-fold more intense for $\mathbf{HL}^{I}$ and about 4-fold more intense for $\mathbf{HL}^{tBuI}$. Another band attributed to the C═N groups is observed at 320 nm for $\mathbf{HL}^{I}$ and shifts to 332 nm in $\mathbf{HL}^{tBuI}$. In both imines and amines, the bands of lowest energies are red-shifted by insertion of *tert*-butyl groups to the phenolate ring.

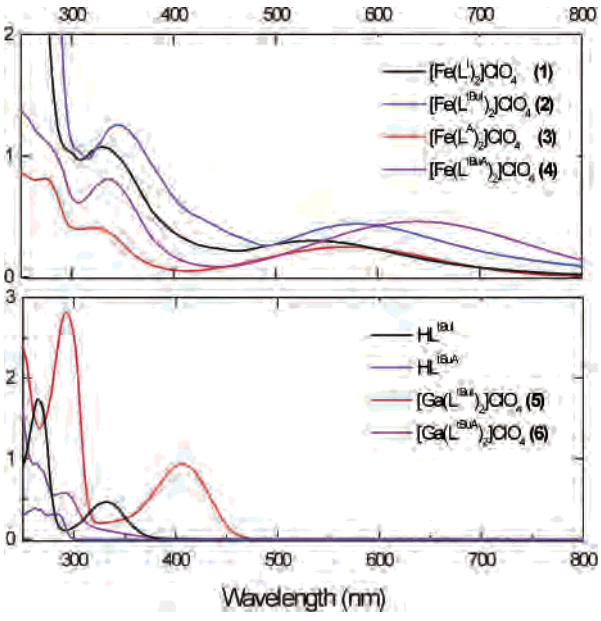

Figure 3. UV−visible spectra of **1**−**6** in dichloromethane, 1.0×10^{-4} M.

The electronic spectra of complexes **1**−**6** were carried out in order to assess the mutual influence between metals and ligands. The iron(III) ion is positioned in a heavily distorted pseudo-octahedral $N_2N'_2O_2$ environment and exhibits a high-spin $3d^5$ configuration, as confirmed by X-ray crystallography and EPR spectroscopy. Thus, ignoring the orientation of the aryl rings, a C_{2v} symmetry arises and this configuration is described as [a_2^1, b_1^1, b_2^1, a_1^1, a_1^1], where a_2, b_1 and b_2 are the d_{xy}, d_{xz}, and d_{yz} orbitals. Since the binary products for a totally symmetric representation in this group are given by $x^2 + y^2 + z^2$, the orbitals $d_{x^2-y^2}$ and d_{z^2} transform as two a_1. Lack of an inversion center implies that relaxing the LaPorte selection rule and increased intensity of the d−d bands is expected, but more intense charge-transfer bands dominate the electronic spectra. Two absorption peaks around 340 and 600 nm are seen for **1**−**4**. Transitions $p\pi_{phenolate} \rightarrow d\pi^*_{iron(III)}$ are associated to the band at around 600 nm, whereas the higher-energy absorption at 340 nm is attributed to a $p\pi_{phenolate} \rightarrow d\sigma^*_{iron(III)}$ LMCT process.[28−30] The potential electronic and steric properties were also analyzed, i.e., σ-donating capability and bulkiness, of the *tert*-butyl groups in the phenolate ring. Unsubstituted **1** shows two bands at 330 and 536 nm that shift bathochromically to 334 and 582 nm for substutited **2**. The amine complex **3** shows bands at 274, 323, and 572 nm in dichloromethane and at 274, 322, and 572 nm in acetonitrile. These results are comparable with those observed for $[Fe^{III}(bbpen)]NO_3 \cdot CH_3OH$ in acetonitrile,[26a]

Table 3. UV−Visible Data for Ligands and Complexes **1**−**6**

	λ (nm)/ ϵ (Lmol^{-1}cm^{-1})[a]
$\mathbf{HL}^{I}$	262 (9500); 284 (2300); 320 (2100)
$\mathbf{HL}^{tBuI}$	264 (17 000); 332 (4500)
$\mathbf{HL}^{A}$	262 (4500); 268 (4350); 278 (3150); 332 (190)
$\mathbf{HL}^{tBuA}$	262 (3750); 268 (3550); 282 (2990)
$[Fe(\mathbf{L}^{I})_2]^+$ **(1)**	236 (37 500); 330 (11 450); 536 (3200)
$[Fe(\mathbf{L}^{tBuI})_2]^+$ **(2)**	278 (39 700); 344 (12 500); 582 (4400)
$[Fe(\mathbf{L}^{A})_2]^+$ **(3)**	274 (7960); 323 (3920); 572 (2420)
$[Fe(\mathbf{L}^{tBuA})_2]^+$ **(4)**	254sh (∼13 400); 276sh (11 100); 336 (8000); 638 (4600)
$[Ga(\mathbf{L}^{tBuI})_2]^+$ **(5)**	292 (58 615); 406 (9470)
$[Ga(\mathbf{L}^{tBuA})_2]^+$ **(6)**	244 (19 200); 262 (9400); 290 (5800)

[a] All solutions are 1.0×10^{-4} M in dichloromethane. All counterions are perchlorate.

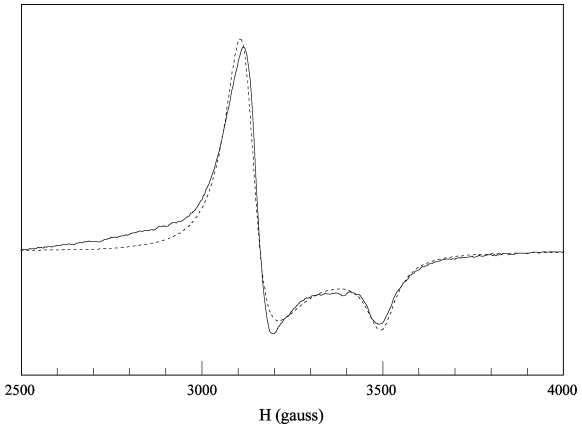

Figure 4. Simulation (···) of the experimental spectrum (—) observed for **2** at g ≈ 2.0.

thus reinforcing the identity of **3**. The bands found at 323 and 572 nm in **3** shift, respectively, to 336 and 638 nm in **4**. The latter band shifts 66 nm upon inclusion of the *tert*-butyl groups, and an increased electron-donating capacity of the phenolate rings is expected.[31] Since the shift is less pronounced for the $p\pi_{phenolate} \rightarrow d\sigma^*_{iron(III)}$ than the $p\pi_{phenolate} \rightarrow d\pi^*_{iron(III)}$ process, these changes were attributed mainly to the bulkiness of the *tert*-butyl groups. These bulky groups may affect the $Fe-O-C_{phenolate}$ angle in **2** and **4**, thus changing the extent of interaction between the $p_{in-plane}$ and $p_{out-of-plane}$ orbitals of the oxygen and the metallic d orbitals.[25a] Neither ligand field nor charge-transfer bands are expected for **5** or **6**, and the trends observed for the ligands are maintained after coordination.

5. EPR Spectroscopy. Selected iron and gallium compounds had their EPR spectra measured. The complexes $[Fe^{III}(L^{tBuI})_2]ClO_4$ **(2)** and $[Fe^{III}(L^{tBuA})_2]ClO_4 \cdot CH_3OH$ **(4)** show features at about $g = 8.0$ and 4.3, thus supporting the high-spin nature of the complexes. Nonetheless, the imine complex **2** shows an additional asymmetric peak at $g \approx 2.0$, as seen in Figure 4.

Since the most remarkable difference between the **2** and **4** is the presence of a C=N bond per ligand in the former complex, the spectra for both compounds was simulated. The spin Hamiltonian $H = \beta_e \hat{S} g B + D[\hat{S}_z^2 - (35/12)] + E[\hat{S}_x^2 - \hat{S}_y^2]$ was used, where D and E are zero-field parameters and the g factor was kept as 2.0. By definition $|E| \leq |D|/3$ for these spectra, and it was assumed that D and E were positive.[32] It is well established[33] that the signal at $g = 4.0$ is only prominent when E is close to $D/3$ and D is equal to or larger than the magnitude of the Zeeman energy (0.3 cm^{-1}). Therefore, spectra were simulated[34] in which $D = 0.2$, 0.3, 0.4, and 0.5 cm^{-1}, with $E/D = 1/3$, 1/4, and 1/5. As the D value gets larger, nothing appears in the $g = 2.0$ region that could support the signal observed for **2** as belonging to a high-spin iron(III) center, and at lower D values, the signal at $g = 4$ distorts and disappears. In terms of the signals at $g = 4$ and 8, the simulation indicates that $E \approx D/3$. Although not a perfect match, the simulation determines the parts of the spectrum belonging to the iron(III) ion. Therefore, the signal at $g = 2$ is assigned to a different paramagnetic species. Simulation of this signal reinforces that this is an isolated spectrum simulated as an $S = {}^1/_2$ species with $g_{||} = 1.93$ and $g_\perp = 2.15$, thus in an axial site symmetry and related to a transition metal ion. We conclude that, due to a differentiated rigidity, compound **2** presents some degree of spin admixture, supporting an equilibrium between a largely predominant $S = 5/2$ from $Fe(III)_{high-spin}$ and an $S = 1/2$ from a minor component $Fe(III)_{low-spin}$ species.[35] As expected, the gallium species are EPR silent.

6. Electrochemistry. Phenoxyl radicals—from Altwicker's work[36] to bioinorganic[37] and magnetic materials[38]—figure among the best-characterized radical systems. It is accepted that *tert*-butyl groups lower the oxidation potential and suppress bimolecular decay reactions at the ring.[39] Therefore, the redox behavior of **1** and **3** was compared to that of **2** and **4**, and gallium-containing **5** and **6**. Ligands and complexes were studied in dichloromethane and acetonitrile. The results are summarized in Table 4, and three representative cyclic voltammograms are displayed in Figure 5.

6.1. The Ligands. An ill-defined irreversible oxidation was observed in dichloromethane for $\mathbf{HL}^{I}$ and $\mathbf{HL}^{A}$, whereas

(27) (a) Brown, M. A.; El-Hadad, A. A.; McGarvey, B. R.; Sung, R. C. W.; Trikha, A. K.; Tuck, D. G. *Inorg. Chim. Acta* **2000**, *300*−*302*, 613. (b) Camacho-Camacho, C.; Merino, G.; Martínez-Martínez, F. J.; Nöth, H.; Contreras, R. *Eur. J. Inorg. Chem.* **1999**, *06*, 1021. (c) Wong, E.; Caravan, P.; Liu, S.; Rettig, S. J.; Orvig, C. *Inorg. Chem.* **1996**, *35*, 715. (d) Beckmann, U.; Bill, E.; Weyhermüller, T.; Wieghardt, K. *Eur. J. Inorg. Chem.* **2003**, *09*, 1768. (e) Darensbourg, D. J.; Billodeaux, D. R. *C. R. Chim.* **2004**, *07*, 755. (f) Van Aelstyn, M. A.; Keizer, T. S.; Klopotek, D. L.; Liu, S.; Munoz-Hernandez, M.-A.; Wei, P.; Atwood, D. A. *Organometallics* **2000**, *19*, 1796. (g) Munoz-Hernandez, M.-A.; Keizer, T. S.; Parkin, S.; Patrick, B.; Atwood, D. A.; *Organometallics* **2000**, *19*, 4416. (h) Wong, E.; Liu, S.; Rettig, S.; Orvig, C. *Inorg. Chem.* **1995**, *34*, 3057.
(28) Glaser, T. Z. *Anorg. Allg. Chem.* **2003**, *629*, 2274.
(29) Karpishin, T. B.; Gebhard, M. S.; Solomon, E. I.; Raymond, K. N. *J. Am. Chem. Soc.* **1991**, *113*, 2977.
(30) Davis, M. I.; Orville, A. M.; Neese, F.; Zaleski, J. M.; Lipscomb, J. D.; Solomon, E. I. *J. Am. Chem. Soc.* **2002**, *124*, 602.
(31) Auerbach, U.; Eckert, U.; Wieghardt, K.; Nuber, B.; Weiss, J. *Inorg. Chem.* **1990**, *29*, 938.
(32) The values of D and E can be considered positive for powder spectra because the relative signs of D and E are related to the assignment of the coordinates x and y, which are not relevant here. The sign of D is important only when $kT \approx D$, and for compounds **2** and **7**, $kT \approx 70$ cm^{-1}.
(33) Mabbs, F. E.; Collison, D. *Electron Paramegnetic Resonance of d Transition Metal Compounds*; Elsevier: Amsterdam, 1992.
(34) The simulations for the Fe^{3+} ion were done with a program provided by Dr. Hogni Weihe, Department of Chemistry, University of Copenhagen, Universitetsparken 5, DK 2100 Copenhagen, Denmark. The simulation of the low-spin signal for the same ion was performed using a program developed by Prof. B. McGarvey.
(35) The apparent axial symmetry of the $Fe(III)_{low-spin}$ species in the EPR signal does not denote an axial site symmetry for the species since the orbitals occupied by the unpaired electron are affected only by π interactions with the ligand. See McGarvey, B. R.; Batista, N. C.; Bezerra, C. W. B.; Schultz, M. S.; Franco, D. W. *Inorg. Chem.* **1998,** *37*, 2865.
(36) Altwicker, E. R. *Chem. Rev.* **1967**, *67*, 475.
(37) (a) Chaudhuri, P.; Wieghardt, K. *Prog. Inorg. Chem.* **2001**, *50*, 151. (b) Jadzewski, B. A.; Tolman, W. B *Coord. Chem. Rev.* **2000**, *200*−*202*, 633.
(38) (a) Schultz, D. A. *Magnetic Properties of Organic Materials*; Lahti, P. M., Ed.; Marcel Dekker: New York, 1999; p 103. (b) Schultz, D. A. *Magnetic Properties of Organic Materials*; Lahti, P. M., Ed.; Marcel Dekker: New York, 1999; p 661.
(39) (a) Snodin, M. D.; Ould-Moussa, L.; Wallmann, U.; Lecomte, S.; Bachler, V.; Bill, E.; Hummel, H.; Weyhermuller, T.; Hildebrandt, P.; Wieghardt, K. *Chem. Eur. J.* **1999**, *05*, 2554. (b) Schnepf, R.; Sokolowski, A.; Mueller, J.; Bachler, V.; Wieghardt, K.; Hildebrandt, P. *J. Am. Chem. Soc.* **1998**, *120*, 2352.

Table 4. Electrochemical Parameters for Ligands and Complexes **1**−**6**[a]

	solvent	$E_{1/2}^1$; (ΔE)[b] in V	$E_{1/2}^2$; (ΔE) in V	$E_{1/2}^3$; (ΔE) in V
HL^{I}	CH_2Cl_2		irreversible behavior	
HL^{tBuI}	CH_2Cl_2	−	0.46 (0.25)	0.97 (ox.)
HL^{A}	CH_2Cl_2		irreversible behavior	
HL^{tBuA}	CH_2Cl_2	−	0.33 (0.19)	0.84 (0.39)
$[Fe(\mathbf{L}^{I})_2]^+$ **(1)**	CH_3CN	−0.73 (0.07)	0.90 (ox)	1.22 (ox)
	CH_2Cl_2	−0.79 (0.07)	−	−
$[Fe(\mathbf{L}^{tBuI})_2]^+$ **(2)**	CH_3CN	−0.88 (0.07)	0.77 (0.07)	1.14 (ox)
	CH_2Cl_2	−0.97 (0.07)	0.69 (0.09)	1.20 (ox)
$[Fe(\mathbf{L}^{A})_2]^+$ **(3)**	CH_3CN	−0.75 (0.19)	0.89 (ox)	−
	CH_2Cl_2	−0.81 (0.40)	−	−
$[Fe(\mathbf{L}^{tBuA})_2]^+$ **(4)**	CH_3CN	−1.03 (0.11)	0.64 (0.10)	0.94 (0.14)
	CH_2Cl_2	−1.11 (0.12)	0.61 (0.11)	0.93 (0.20)
$[Ga(\mathbf{L}^{tBuI})_2]^+$ **(5)**	CH_3CN	−	0.78 (0.08)	1.07 (ox)
	CH_2Cl_2	−	0.78 (0.07)	1.08 (0.25)
$[Ga(\mathbf{L}^{tBuA})_2]^+$ **(6)**	CH_3CN	−	0.62 (0.07)	0.79 (0.15)
	CH_2Cl_2	−	0.60 (0.10)	0.85 (0.10)

[a] The couple Fc^+/Fc presents ΔE ($=E_{pc} - E_{pa}$) = 0.12 V in dichloromethane and 0.07 V in acetonitrile; thus, we consider processes exhibiting ΔE between 0.06 and 0.12 V as being reversible, 0.12 and 0.15 V as being quasi-reversible, and processes wider than 0.15 V as irreversible.

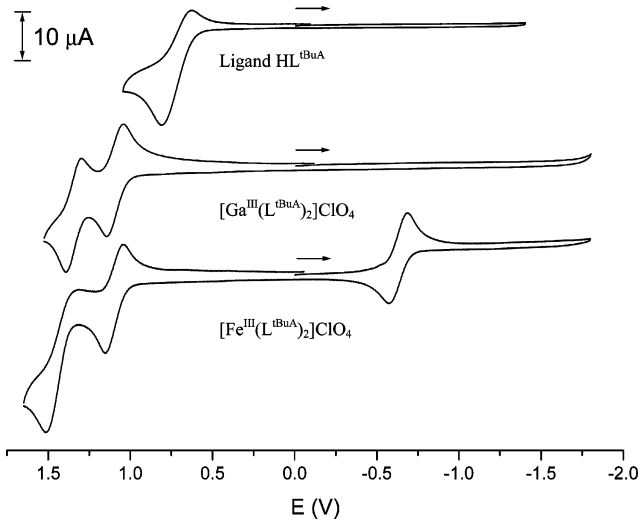

Figure 5. Cyclic voltammograms of **HL**^{tBuA}, **4**, and **6** in dichloromethane.

a quasi-reversible behavior to the formation of a phenoxyl radical species was observed for **HL**^{tBuI} at 0.46 V vs Fc^+/Fc. An irreversible oxidation was also observed at 0.97 V vs Fc^+/Fc. These results are in excellent agreement with the phenol−imidazole proligand **LH** of Benisvy et al.,[40] who postulate that extra stabilization of the cationic radical species is achieved by hydrogen bonding. Indeed, **HL**^{tBuI} has a rigid framework that allows the O_{phenol}−H···N_{imine} interaction to take place. A similar behavior is observed for **HL**^{tBuA} at 0.33 vs Fc^+/Fc and attributed to the couple [**HL**^{tBuA}]/ [**HL**^{tBuA}]$^{\bullet+}$. The decreased potential can be associated to a less-stable hydrogen bonding due to a flexible framework.

6.2. Gallium Complexes. Trivalent gallium is redox-inactive, and **5** and **6** were included as probes for electroactive ligands.[41] No metal-centered redox activity was observed, and the reversible processes observed in dichloromethane at 0.78 V for **5** and 0.62 V vs Fc^+/Fc for **6** are attributed to the formation of phenoxyl radicals. It demonstrates an enhancement in the electroactivity of the ligands upon coordination. Compound **5** appears uninfluenced by solvent effects, but **6** is more susceptible to such changes, and the second process shifts from 0.79 V vs Fc^+/Fc in dichloromethane to 0.85 V vs Fc^+/Fc in acetonitrile. One can speculate that upon the formation of the radical species a much weaker interaction between the double-bonded oxygen atom of the phenoxyl rings and the metal leads to a solvent-dependent rearrangement of the ligands. A rigid ligand as in **5** minimizes such effects.

6.3. Iron Complexes. Compounds **1**−**4** had their redox properties analyzed. A single process is observed for **1** and **3** at ca. −0.75 V vs Fc^+/Fc in acetonitrile, being attributed to the redox couple Fe^{III}/Fe^{II}. This process is irreversible for **3** in dichloromethane, and ill-defined oxidations characterize the ligand-centered activity in both solvents. The CV of **2** in acetonitrile shows the Fe^{III}/Fe^{II} couple at −0.88 V vs Fc^+/Fc, followed by reversible and ill-defined ligand-centered oxidations at 0.77 and 1.14 V vs Fc^+/Fc, respectively. Similar behavior is observed in dichloromethane. Quasi-reversible behavior dominates the redox activity of **4** with waves at −1.03, 0.64, and 0.94 V vs Fc^+/Fc related, respectively, to Fe^{III}/Fe^{II}, and two ligand-centered processes. The Fe^{III}/Fe^{II} process shifts considerably and exclusion of the latter ligand-related process improves considerably the reversibility of the phenolate/phenoxyl couple at 0.64 V vs Fc^+/Fc. This increased reversibility is attributed to the rigid framework of the imine ligand.

Spectroelectrochemical and coulometric experiments followed by EPR spectroscopy were not completely successful due to slow electron transfers. However, the observation of UV−visible peaks around 390 and 440 nm, as well as of an EPR signal at $g = 2.03$ for **4**, along with theoretical calculations serve as a strong evidence for the formation of phenoxyl radicals.[42]

7. Electronic Structure Analysis. A series of electronic structure calculations were carried out to evaluate our

(40) Benisvy, L.; Blake, A. J.; Collison, D.; Davies, E. S.; Garner, C. D.; McInnes, E. J. L.; McMaster, J.; Whittaker, G.; Wilson, C. *Dalton Trans.* **2003**, *10*, 1975.

(41) (a) Adam, B.; Bill, E.; Bothe, E.; Goerdt, B.; Haselhorst, G.; Hildenbrand, K.; Sokolowski, A.; Steenken, S.; Weyhermueller, T.; Wieghardt, K. *Chem. Eur. J.* **1997**, *03*, 308. (b) Sokolowski, A.; Bothe, E.; Bill, E.; Weyhermueller, T.; Wieghardt, K. *Chem. Commun.* **1996**, 1671.

(42) (a) Nairn, A. K.; Bhalla, R.; Foxon, S. P.; Liu, X.; Yellowlees, L. J.; Gilbert, B. C.; Walton, P. H. *Dalton Trans.* **2002**, 1253. (b) Verani, C. N.; Bothe, E.; Burdinski, D.; Weyhermuller, T.; Florke, U.; Chaudhuri, P. *Eur. J. Inorg. Chem.* **2001**, *08*, 2161.

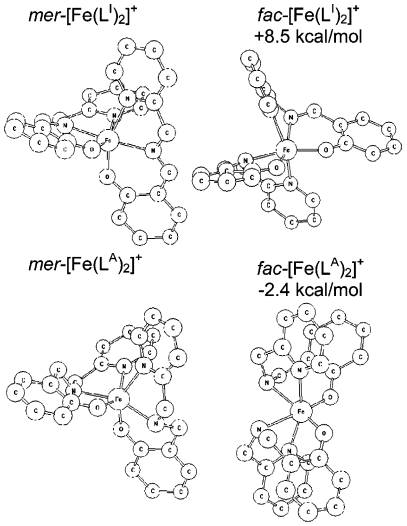

Figure 6. Minimized geometries and energies for *mer*-$[Fe(\mathbf{L}^{I})_2]^+$, *fac*-$[Fe(\mathbf{L}^{I})_2]^+$ *mer*-$[Fe(\mathbf{L}^{A})_2]^+$, and *fac*-$[Fe(\mathbf{L}^{A})_2]^+$. Values in parentheses indicate energies in kcal/mol. H atoms have been omitted for clarity.

explanation for facial and meridional preferences observed experimentally for **1**−**4**. Meridional/facial preferences were investigated by computing differences in energies for the isomeric pairs *mer*- and *fac*-$[Fe(\mathbf{L}^{I})_2]^+$ and *mer*- and *fac*-$[Fe(\mathbf{L}^{A})_2]^+$. Optimized geometries and energies for these structures are depicted in Figure 6 and are in good agreement with the related crystal structures. In agreement with experimental results, *mer*-$[Fe(\mathbf{L}^{I})_2]^+$ is more stable than *fac*-$[Fe(\mathbf{L}^{I})_2]^+$ by 8.5 kcal/mol. For $(\mathbf{L}^{A})^-$, *mer*-$[Fe(\mathbf{L}^{A})_2]^+$ is less stable than *fac*-$[Fe(\mathbf{L}^{A})_2]^+$ by 2.4 kcal/mol. This difference in the coordination modes was attributed to the rigidity of $(\mathbf{L}^{I})^-$, and to test this hypothesis, pyridine and 2-iminomethyl phenolate were used to mimic the electronic interaction of $(\mathbf{L}^{I})^-$ with the iron(III) ion (Figure S1). The results show that the *fac* configuration is more stable by 2.11 kcal/mol, indicating that the meridional preference of $[Fe(\mathbf{L}^{I})_2]^+$ is not due to differences in the electronic structures of $(\mathbf{L}^{I})^-$ and $(\mathbf{L}^{A})^-$. Instead, the meridional coordination is favored by $(\mathbf{L}^{I})^-$ because of the rigidity of the ligand, which accounts for an energy reversal of more than 10 kcal/mol.

Electronic structure methods have also been used to investigate the nature of the oxidation of *mer*-$[Fe(\mathbf{L}^{I})_2]^+$ and *fac*-$[Fe(\mathbf{L}^{A})_2]^+$. The electronic densities for the 1+ and 2+ species (i.e., the starting complexes and their radical-containing oxidized forms, respectively) of both compounds were calculated using the 1+ optimized geometries. Spin density plots in Figure 7 display differences between α and β densities; regions of excess α density are shown in yellow and excess β density are in green. As expected, the spin densities of un-oxidized *mer*-$[Fe(\mathbf{L}^{I})_2]^+$ and *fac*-$[Fe(\mathbf{L}^{A})_2]^+$ indicate large α density at the iron(III) center. In a molecular orbital treatment, oxidation can remove either an α or β electron (the calculated results are qualitatively the same). For clarity, Figure 7 displays the spin densities after removal of an α electron. The plots for *mer*-$[Fe(\mathbf{L}^{I})_2]^{2+}$ and *fac*-$[Fe(\mathbf{L}^{A})_2]^{2+}$ show excess β spin on the phenolate rings, confirming that the α electron was removed from these ligands rather than from the metal. Thus, upon oxidation, radical formation occurs on the phenolate rings.

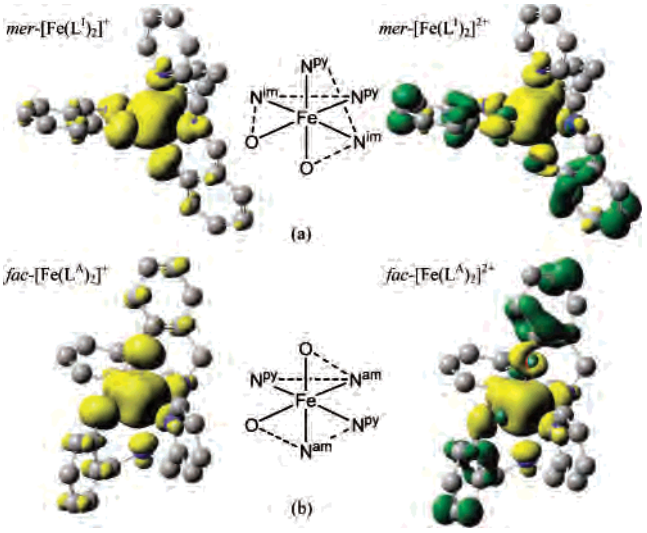

Figure 7. Spin density plots for (a) *mer*-$[Fe(\mathbf{L}^{I})_2]^+$ and *mer*-$[Fe(\mathbf{L}^{I})_2]^{2+}$ and (b) *fac*-$[Fe(\mathbf{L}^{A})_2]^+$ and *fac*-$[Fe(\mathbf{L}^{A})_2]^{2+}$. 2D drawings are also given to show ligand configurations. Yellow indicates excess α electron density, and green indicates excess β electron density.

Conclusions

Asymmetric ligands consisting of the tridentate imines $\mathbf{HL}^{RI}$ and the amines $\mathbf{HL}^{RA}$, R being H or *tert*-butyl groups, were studied as discrete mononuclear molecules in which one metal ion (trivalent iron or gallium) is coordinated by two deprotonated ligands in a distorted $(N_{amine}N_{pyridine}O_{phenolate})_2$ octahedral environment. The results were remarkable: (a) the nature/rigidity of the ligands defines whether meridional or facial coordination will take place, (b) the presence of tertiary butyl groups is pivotal for the formation of phenoxyl radicals, and (c) metal coordination enhances the reversibility of the phenolate/phenoxyl couple. X-ray structures were determined for **2**, **4**, and **6**. Imine ligands coordinate meridionally, while amines prefer facial modes with both R = H and *tert*-butyl. The iron and gallium complexes avoid trans coordination of the phenolate oxygen atoms. Finally, the generation of the complexed phenoxyl-containing species depends on the presence of substituents at the ortho and para positions of the phenolate ring. As evidenced by the data above, unsubstituted phenolates are much less electroactive than those containing bulky electron-donor *tert*-butyl groups.

Acknowledgment. C.N.V. thanks the Wayne State University and the Donors of the Petroleum Research Fund (Grant No. 42575-G3) for financial support. H.B.S. thanks the National Science Foundation (Grant No. CHE 0131157), and H.P.H. thanks the Institute for Scientific Computing at Wayne State University for support provided by an NSF-IGERT fellowship. This work is dedicated to Prof. Ademir Neves.

Supporting Information Available: Crystallographic data; characterization data; and calculated structural coordinates. This material is available free of charge via the Internet at http://pubs.acs.org.

IC050658J